nature communications

Article

https://doi.org/10.1038/s41467-024-50856-2

Conventional superconductivity in the doped kagome superconductor $Cs(V_{0.86}Ta_{0.14})_3Sb_5$ from vortex lattice studies

Received: 9 March 2024

Accepted: 22 July 2024

Published online: 31 July 2024

Check for updates

Yaofeng Xie[1,9], Nathan Chalus[2,9], Zhiwei Wang[3,4,5,9], Weiliang Yao[1], Jinjin Liu[3,4], Yugui Yao[3,4,5], Jonathan S. White[6], Lisa M. DeBeer-Schmitt[7], Jia-Xin Yin[8], Pengcheng Dai[1] & Morten Ring Eskildsen[2]

A hallmark of unconventional superconductors is a complex electronic phase diagram where intertwined orders of charge-spin-lattice degrees of freedom compete and coexist. While the kagome metals such as CsV_3Sb_5 also exhibit complex behavior, involving coexisting charge density wave order and superconductivity, much is unclear about the microscopic origin of the superconducting pairing. We study the vortex lattice in the superconducting state of $Cs(V_{0.86}Ta_{0.14})_3Sb_5$, where the Ta-doping suppresses charge order and enhances superconductivity. Using small-angle neutron scattering, a strictly bulk probe, we show that the vortex lattice exhibits a strikingly conventional behavior. This includes a triangular symmetry with a period consistent with $2e$-pairing, a field dependent scattering intensity that follows a London model, and a temperature dependence consistent with a uniform superconducting gap. Our results suggest that optimal bulk superconductivity in $Cs(V_{1-x}Ta_x)_3Sb_5$ arises from a conventional Bardeen-Cooper-Schrieffer electron-lattice coupling, different from spin fluctuation mediated unconventional copper- and iron-based superconductors.

In conventional Bardeen-Cooper-Schrieffer (BCS) superconductors, the electron-lattice coupling leads to the formation of coherent ($2e$) Cooper pairs and the opening of an isotropic s-wave gap at the Fermi level[1]. In comparison, a key signature of unconventional superconductivity in materials such as copper oxides and iron-pnictides is that the pairing may be mediated by spin fluctuations[2,3] and associated with intertwined charge-spin-lattice degrees of freedom[4]. The discovery of superconductivity in the layered kagome AV_3Sb_5 (A = K, Rb, Cs) metals[5–7] is interesting because the superconducting state develops in the presence of a charge density wave (CDW)[8–13], and the competition between these two ordered states may give rise to unconventional superconductivity[14–18]. However, no spin fluctuations are reported, thus raising the question of whether these materials are conventional BCS or unconventional superconductors like cuprates

[1]Department of Physics and Astronomy, Rice University, Houston, TX, USA. [2]Department of Physics and Astronomy, University of Notre Dame, Notre Dame, IN, USA. [3]Centre for Quantum Physics, Key Laboratory of Advanced Optoelectronic Quantum Architecture and Measurement (MOE), School of Physics, Beijing Institute of Technology, Beijing, China. [4]Beijing Key Lab of Nanophotonics and Ultrafine Optoelectronic Systems, Beijing Institute of Technology, Beijing, China. [5]Material Science Center, Yangtze Delta Region Academy of Beijing Institute of Technology, Jiaxing, China. [6]Laboratory for Neutron Scattering and Imaging (LNS), PSI Center for Neutron and Muon Sciences, Paul Scherrer Institute, Villigen PSI, Switzerland. [7]Large Scale Structures Section, Neutron Scattering Division, Oak Ridge National Laboratory, Oak Ridge, TN, USA. [8]Department of Physics, Southern University of Science and Technology, Shenzhen, China. [9]These authors contributed equally: Yaofeng Xie, Nathan Chalus, Zhiwei Wang. e-mail: eskildsen@nd.edu

and iron pnictides. From pressure and Ta-doping dependence of the $Cs(V_{1-x}Ta_x)_3Sb_5$ phase diagram, it is clear that CDW order competes with superconductivity, and optimal superconductivity of $T_c = 5.3$ K appears around $Cs(V_{0.86}Ta_{0.14})_3Sb_5$ with vanishing CDW order[19,20].

The majority of experimental evidence in the AV_3Sb_5 materials indicates singlet *s*-wave pairing with a nodeless but possibly anisotropic superconducting gap[19,21–23]. Furthermore, multiband superconductivity with a large difference in the gap size on different Fermi surface sheets has been reported[12,15,22–25]. An experimental determination of electron-lattice coupling strength supports conventional BCS superconductivity[26], although there are questions about whether the relation between the gap and critical temperature is consistent with weak coupling[14]. There are several reports of broken time-reversal symmetry (BTRS) both in the normal state[8,27–29] as well as the superconducting state[30–32], although it is not observed consistently in all experiments[23,33,34]. In addition, possible Majorana bound states were observed in scanning tunneling spectroscopy studies[9]. Finally, a transition from conventional 2*e*-pairing towards (vestigial) 4*e*- and 6*e*-pairing[35] has been reported upon heating towards the transition to the normal state[36–40].

To determine the microscopic origin of superconductivity in AV_3Sb_5, it is critical to separate the effects of the CDW as this may be associated with an electronic nematic phase and affect the electron pairing[41,42]. Here, we report on small-angle neutron scattering (SANS) studies of the vortex lattice (VL) induced by an applied magnetic field in $Cs(V_{0.86}Ta_{0.14})_3Sb_5$ where charge ordering is suppressed[19,20]. The vortices produce singularities in the order parameter and may be used as probes of the superconducting state in the host material[43,44]. Our results indicate a highly conventional bulk superconducting state, and thus suggest that the reported exotic behavior in other members of the AV_3Sb_5 family of superconductors are not relevant to the microscopic origin of superconductivity. Importantly, the SANS technique provides information about the bulk superconducting state, whereas more exotic phenomena such as BTRS may occur only at the sample surface.

Results

Vortex lattice imaging

The sample used for the SANS experiments, shown in Fig. 1a, consisted of a mosaic of co-aligned $Cs(V_{0.86}Ta_{0.14})_3Sb_5$ single crystals. Two SANS experiments (#1/2) were performed, exploring different temperature and field ranges as indicated in the phase diagram in Fig. 1b. In all cases, the magnetic field was applied perpendicular to the six-fold symmetric (kagome) lattice planes. Figures 1c–e shows VL diffraction patterns for $Cs(V_{0.86}Ta_{0.14})_3Sb_5$ at three different applied magnetic fields. The system was prepared by a field cooling to the measurement temperature from above T_c, followed by a damped field oscillation with an initial amplitude of 5% of the measurement field. As witnessed by the well-defined defined Bragg peaks, this produces an ordered VL, which is consistent with weak pinning[45].

A triangular VL is observed at all fields and temperatures as expected for a superconductor with a six-fold symmetric basal plane, and oriented with Bragg peaks along the $[\bar{1}\,2\,0]$ crystalline direction. The same symmetry and orientation is observed in a reference measurement on undoped CsV_3Sb_5 as shown in Fig. 1f, although VL imaging is only possible at a low field and temperature due to the much larger penetration depth (182.7 nm vs 106.8 nm) and much lower upper critical field (0.3 T vs 2.2 T)[46]. In contrast, vortex imaging by scanning tunneling spectroscopy (STS) found a VL that undergoes a 15° rotation

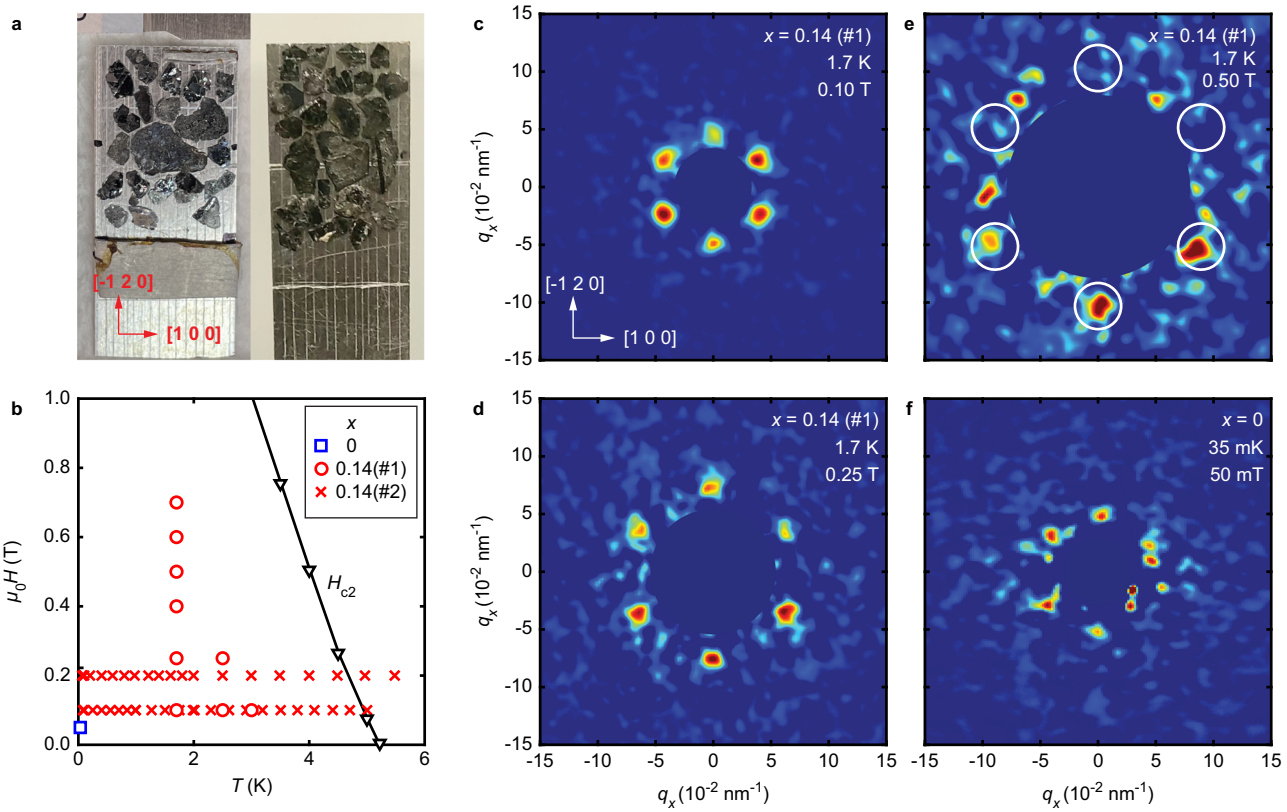

Fig. 1 | Vortex lattice diffraction patterns. a $Cs(V_{0.86}Ta_{0.14})_3Sb_5$ sample mosaic used for the SANS experiments, with the arrows indicating the in-plane crystalline directions. **b** Field-temperature phase diagram indicating where SANS were performed. **c** $Cs(V_{0.86}Ta_{0.14})_3Sb_5$ VL diffraction pattern at 1.7 K and 0.1 T. The arrows indicate the crystalline orientation. **d** Same at 0.25 T and **e** 0.5 T. In panel (**e**) only Bragg peaks at the lower half of the detector were rocked through the Ewald sphere and the positions of symmetry equivalent peaks are indicated by circles. **f** CsV_3Sb_5 VL diffraction pattern at 35 mK and 50 mT. For all diffraction patterns, background measurements obtained at zero field are subtracted and the region near $q = 0$ is masked off. A separate color scale is used for each diffraction pattern.

https://doi.org/10.1038/s41467-024-50856-2

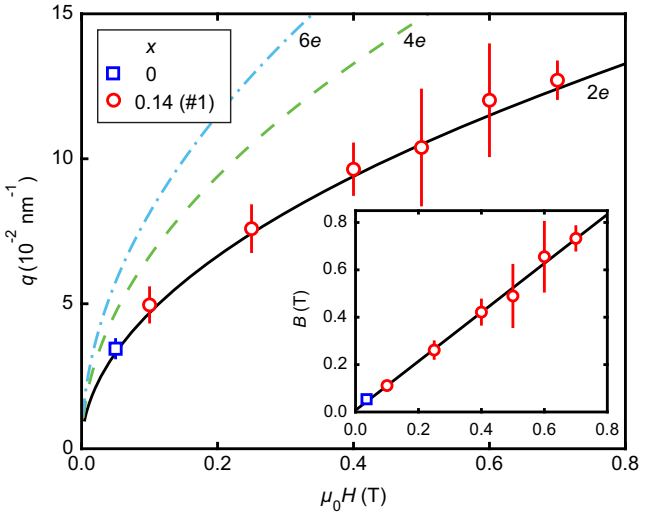

Fig. 2 | Field dependence of the vortex lattice scattering vector. Full, dashed and dot-dashed lines indicate q expected for 2e, 4e and 6e-pairing respectively. Inset shows the magnetic induction determined from eqn. (1) assuming 2e-pairing. The line is a linear fit. Data for $x = 0.14$ was measured at 1.7 K and for $x = 0$ at 35 mK. For both the main figure and the inset, error bars represent one standard deviation.

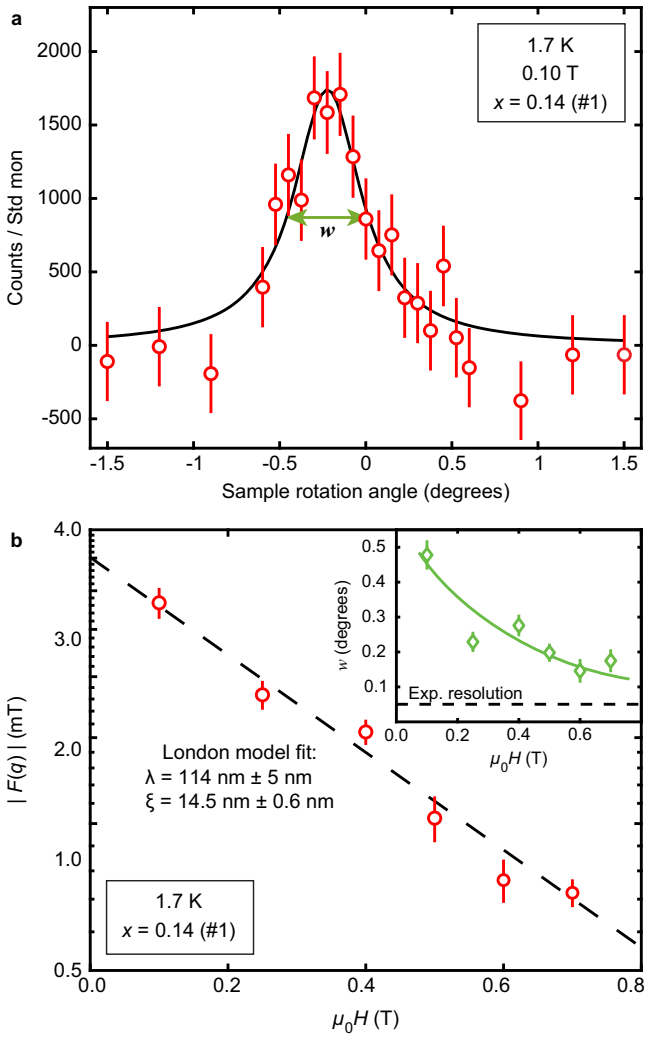

Fig. 3 | Vortex lattice form factor. a Scattered intensity as the VL Bragg is rotated through the Ewald sphere. The curve is a Lorentzian fit and the full-width-half-maximum (w) is indicated by the arrow. **b** VL form factor versus applied magnetic field. The dashed line is a fit to eqn. (3), with the penetration depth and coherence length indicated in the plot. Inset shows the full-width-half-maximum rocking curve widths obtained from Lorentzian fits. The solid line is a guide to the eye and the dashed line shows the experimental resolution. For all panels, error bars indicate one standard deviation.

as the applied field is increased from 75 mT to 200 mT, and where the high field orientation is orthogonal to the one reported here[47]. This highlights how different results, reflecting the bulk properties, may be obtained using SANS compared to surface probes with a limited field of view, such as STS.

The VL orientation is determined by anisotropies within the screening current plane, which may arise from the Fermi surface (FS)[48] or the superconducting gap[49–51]. Considering reports of an isotropic gap on all three FS sheets in $Cs(V_{0.86}Ta_{0.14})_3Sb_5$[19], the former scenario is the most likely. A direct correlation between the VL orientation and the band structure requires an evaluation of Fermi velocity averages as well as a directionally resolved Density of States at the Fermi level[48,52], which has presently not been carried out for CsV_3Sb_5 or $Cs(V_{0.86}Ta_{0.14})_3Sb_5$. Nevertheless, the morphology of almost perfectly nested hexagonal (β) and triangular (δ) FS sheets with flat sections perpendicular to the Γ-K direction[13,19,53,54], is consistent with the observed VL orientation. This commonality, together with the isotropic (α) FS sheet, may also explain the absence of a field-driven VL rotation transition observed in other multiband superconductors such as MgB_2[55] and UPt_3[56,57].

Scattering vector magnitude

The scattering vector magnitude for a triangular VL is

$$q_{ne}(B) = 2\pi\sqrt{\frac{2B}{\sqrt{3}\Phi_{ne}}}, \quad (1)$$

where B is the magnetic induction, $\Phi_{ne} = h/ne$ is the flux quantum and n is an even integer. For regular 2e-pairing the flux quantum is given by $\Phi_{2e} = \Phi_0 = 2068\ \mathrm{Tnm}^2$ [58]. Figure 2 shows the measured VL scattering vector (q) versus applied magnetic field ($\mu_0 H$). This follows the behavior expected for 2e-pairing, assuming $B = \mu_0 H$. Furthermore, q can be reliably determined at temperatures up to $\sim \frac{2}{3} T_c$ at 0.1 T and shows no deviation from q_{2e}. In contrast, q_{4e} and q_{6e} are not compatible with the data within the experimental error. While agreement could in principle be achieved for $n \neq 2$, it requires $B = \sqrt{n/2}\,\mu_0 H$ which is inconsistent with magnetization measurements on $Cs(V_{0.86}Ta_{0.14})_3Sb_5$[46]. The SANS results do thus not provide evidence for 4e- and 6e-pairing at the bulk level that has been reported for CsV_3Sb_5 as one approaches T_c[39]. The inset to Fig. 2 shows the magnetic induction inferred from the measured q and using eqn. (1) with $n = 2$. A linear fit to the data yields a slope of 1.033 ± 0.015 and an ordinate intercept of $B = 7.4\ \mathrm{mT} \pm 4.2\ \mathrm{mT}$. The latter provides an upper limit of a few milliTesla on any net spontaneous field.

Form factor field dependence

The field dependence of the scattered intensity provides information about the superconducting penetration depth (λ) and coherence length (ξ). This requires a measurement of the integrated intensity, obtained by rotating the VL diffraction peak through the Bragg condition as shown in Fig. 3a. Normalizing by the incident neutron flux one obtains the VL reflectivity

$$R = \frac{2\pi\gamma_n^2\lambda_n^2 t_s}{16\Phi_{ne}^2 q}|F(q)|^2, \quad (2)$$

where $F(q)$ is the VL form factor, $\gamma_n = 1.913$ is the neutron magnetic moment in units of the nuclear magneton, and t_s is the sample thickness[59,60]. Figure 3(b) shows the form factor obtained from the SANS measurement which is found to decrease exponentially with

https://doi.org/10.1038/s41467-024-50856-2

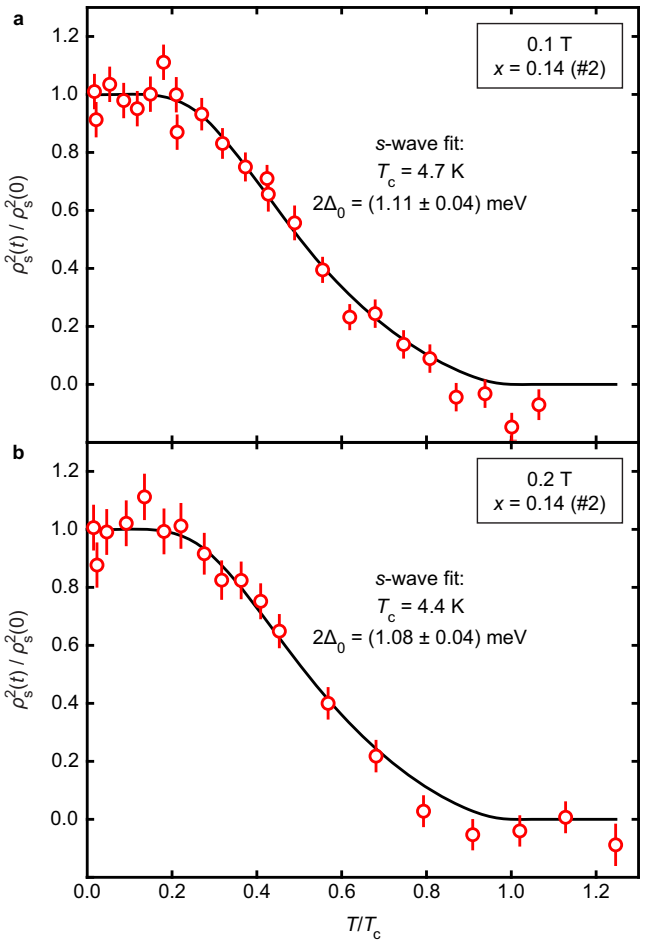

Fig. 4 | Temperature dependence of the superfluid density. a 0.1 T and **b** 0.2 T. Error bars indicate one standard deviation. The curves are fits to an *s*-wave model as described in the text, with gap values and critical temperatures indicated in the plots.

increasing field. This is consistent with the London model

$$F(q) = \frac{B}{1+q^2\lambda^2}\, e^{-q^2\xi^2/2}, \tag{3}$$

with a Gaussian core cut-off to account for a finite coherence length[61,62]. The numerical factor of $\frac{1}{2}$ in the exponent has been found to yield reasonable values for the coherence length in a range of superconductors, although other values have been used in the literature[43]. For $q\lambda \gg 1$ the only field dependence is through $q^2 \propto B$ in the exponent. A fit to the data yields $\lambda = (113.7 \pm 4.8)$ nm from the zero field intercept, and $\xi = (14.5 \pm 0.6)$ nm from the slope. This agrees well with values for $\lambda = 106.8$ nm and $\xi = 12.2$ nm inferred from measurements of the lower and upper critical fields[46]. Notably, the data in Fig. 3b shows no deviation from a purely exponential behavior which may arise from multiband superconductivity[55] or Pauli paramagnetic effects effects[63–65].

The rocking curve width (w) is inversely proportional to the longitudinal VL correlation length. As shown in the Fig. 3b inset, w decreases with increasing field, approaching the experimental resolution. This gradual ordering is commonly observed in superconductors with low pinning and attributed to an enhanced vortex-vortex interactions, and resulting increasing VL tilt modulus, as the density increases[66]. This provides additional support for weak vortex pinning previous reported for $Cs(V_{0.86}Ta_{0.14})_3Sb_5$[46].

Temperature dependence of scattering intensity

The form factor is proportional to the superfluid density (ρ_s), which is dominated by the lowest gap values for a reduced temperature $t = T/T_c \lesssim \frac{1}{3}$. Figure 4 shows the normalized superfluid density versus temperature for two different applied fields, which display a clear saturation as $t \to 0$. In the simplest case of an *s*-wave superconductor with a uniform gap

$$\rho_s(t) = 1 - \frac{1}{2t}\int_0^\infty \cosh^{-2}\left(\frac{\sqrt{\varepsilon^2+\Delta^2(t)}}{2t}\right) d\varepsilon, \tag{4}$$

where $\Delta(t)$ is the temperature-dependent superconducting gap in units of k_BT_c[67]. In the weak coupling limit

$$\Delta(t) = \Delta_0 \tanh\left(\frac{\pi}{\Delta_0}\sqrt{\frac{1}{t}-1}\right), \tag{5}$$

and Δ_0 is the zero-temperature gap amplitude[68]. Curves in Fig. 4 show fits to the SANS data across the entire measured temperature range, using eqs. (4) and (5) and the measured values for T_c. This yields a superconducting gap of $2\Delta_0 = (1.11 \pm 0.04)$meV (0.1 T) and (1.08 ± 0.04) meV (0.2 T) or $2\Delta_0/k_BT_c = 2.74 \pm 0.09$ and 2.85 ± 0.11 respectively, somewhat lower than the BCS prediction of 3.53 and confirming weak coupling superconductivity. This is consistent with the uniform gap across all FS sheets obtained from ARPES[19], although our values are roughly 25% smaller. Estimates of the gap obtained from $\rho_s(t)$ determined by measurements of the lower critical field for $T \geq \frac{1}{3}T_c$ yielded an even larger gap, $2\Delta_0 = (3.6 \pm 0.8)$meV[46]. We note that a uniform (nodeless) gap does not preclude e.g., $s \pm is$ pairing that would break time-reversal symmetry or multiband superconductivity with a s^{++} or s^{+-} state[69], but is inconsistent with *d*-wave or *p*-wave pairing.

In summary, our SANS studies of the $Cs(V_{0.86}Ta_{0.14})_3Sb_5$ VL indicates a wholly conventional superconducting state. Furthermore, the optimal superconductivity without CDW order is likely a conventional BCS superconductor, where electron pairing is induced by electron-lattice coupling. Our results on $Cs(V_{0.86}Ta_{0.14})_3Sb_5$ thus suggest that the exotic properties reported for CDW related phenomena in other members of the AV_3Sb_5 superconductors are likely not related to the microscopic origin of superconductivity.

Methods

Single crystals of $Cs(V_{1-x}Ta_x)_3Sb_5$ were grown by by the self-flux method[5,19,70,71]. These materials form in a layered kagome structure with a *P6/mmm* space group[5], and with facets that allow for an easy determination of the in-plane crystalline axes. For the SANS measurements a mosaic of co-aligned $Cs(V_{0.86}Ta_{0.14})_3Sb_5$ single crystals with a critical temperature $T_c = 5.3$ K and a total mass of 200 mg was used, oriented with the [1 0 0]-axis horizontal and the $[\bar{1}\,2\,0]$-axis vertical. The co-alignment of the individual crystals in the mosaics is confirmed by the six sharp VL Bragg peaks observed in Figs. 1c–f and the absence of significant scattered intensity in between those. This also excludes twinning within the single crystals.

The SANS measurements were carried out using the SANS-I instrument at the Swiss Spallation Neutron Source (SINQ) at the Paul Scherrer Institute. Two experiments were performed, using a pumped ^{4}He cryomagnet for measurements down to 1.7 K (#1) or a dilution refrigerator (DR) for measurements between 67 mK and T_c (#2). A reference measurement was performed on a mosaic of undoped CsV_3Sb_5 sample (280 mg, $T_c = 3.0$ K) using the GP-SANS instrument at the High Flux Isotope Reactor (HFIR) at Oak Ridge National Laboratory (ORNL). These measurements were carried out at a temperature of 35 mK using a DR.

In all cases, a neutron wavelength $\lambda_n = 1.4$ nm and bandwidth of $\Delta\lambda_n/\lambda_n = 10\%$ was used, and the diffracted neutrons were detected

using a position-sensitive detector placed at 11 m from the sample. The horizontal magnetic field was applied along the crystalline [0 0 1]-direction and near-parallel to the incident neutron beam. The sample and cryomagnet were rotated together about the horizontal axes perpendicular to the beam direction to satisfy the Bragg condition for the different VL peaks. Small-angle background measurements were collected in zero field at the base temperature for the respective experiment, and subtracted from the data.

All SANS data was analyzed using the GRASP graphical reduction and analysis software for small-angle neutron scattering available at https://www.ill.fr/grasp/[72].

Data availability

Raw data were generated at the Swiss Spallation Neutron Source SINQ and at the High Flux Isotope Reactor large-scale facilities, and access will be granted upon request. Derived data presented in Figs. 1(b), 2, 3, and 4 is available through Figshare[73].

References

1. Bardeen, J., Cooper, L. N. & Schrieffer, J. R. Theory of superconductivity. *Phys. Rev.* **108**, 1175–1204 (1957).
2. Scalapino, D. J. A common thread: the pairing interaction for unconventional superconductors. *Rev. Mod. Phys.* **84**, 1383–1417 (2012).
3. Dai, P. Antiferromagnetic order and spin dynamics in iron-based superconductors. *Rev. Mod. Phys.* **87**, 855–896 (2015).
4. Fradkin, E., Kivelson, S. A. & Tranquada, J. M. Colloquium: theory of intertwined orders in high temperature superconductors. *Rev. Mod. Phys.* **87**, 457–482 (2015).
5. Ortiz, B. R. et al. CsV_3Sb_5: A Z_2 Topological kagome metal with a superconducting ground state. *Phys. Rev. Lett.* **125**, 247002 (2020).
6. Jiang, K. et al. Kagome superconductors AV_3Sb_5 (A = K, Rb, Cs). *Natl. Sci. Rev.* **10**, nwac199 (2022).
7. Wilson, S. D. & Ortiz, B. R. AV_3Sb_5 kagome superconductors. *Nat. Rev. Mater.* **9**, 420–432 (2024).
8. Jiang, Y.-X. et al. Unconventional chiral charge order in kagome superconductor KV_3Sb_5. *Nat. Mater.* **20**, 1353–1357 (2021).
9. Liang, Z. et al. Three-dimensional charge density wave and surface-dependent vortex-core states in a kagome superconductor CsV_3Sb_5. *Phys. Rev. X* **11**, 031026 (2021).
10. Li, H. X.et al. Observation of unconventional charge density wave without acoustic phonon anomaly in kagome superconductors AV_3Sb_5 (A = Rb,Cs). *Phys. Rev.* **11**, 031050 (2021).
11. Zhao, H. et al. Cascade of correlated electron states in the kagome superconductor CsV_3Sb_5. *Nature* **599**, 216–221 (2021).
12. Chen, H. et al. Roton pair density wave and unconventional strong-coupling superconductivity in a topological kagome metal. *Nature* **599**, 222–228 (2021).
13. Kang, M. et al. Twofold van Hove singularity and origin of charge order in topological kagome superconductor CsV_3Sb_5. *Nat. Phys.* **18**, 301–308 (2022).
14. Tan, H., Liu, Y., Wang, Z. & Yan, B. Charge density waves and electronic properties of superconducting kagome metals. *Phys. Rev. Lett.* **127**, 046401 (2021).
15. Xu, H.-S. et al. Multiband superconductivity with sign-preserving order parameter in kagome superconductor CsV_3Sb_5. *Phys. Rev. Lett.* **127**, 187004 (2021).
16. Song, Y. et al. Competition of superconductivity and charge density wave in selective oxidized CsV_3Sb_5 Thin Flakes. *Phys. Rev. Lett.* **127**, 237001 (2021).
17. Chen, Q., Chen, D., Schnelle, W., Felser, C. & Gaulin, B. D. Charge density wave order and fluctuations above T_{CDW} and below superconducting T_c in the kagome metal CsV_3Sb_5. *Phys. Rev. Lett.* **129**, 056401 (2022).
18. Kang, M. et al. Charge order landscape and competition with superconductivity in kagome metals. *Nat. Mater.* **22**, 186–193 (2023).
19. Zhong, Y. et al. Nodeless electron pairing in CsV_3Sb_5-derived kagome superconductors. *Nature* **617**, 488–492 (2023).
20. Xiao, Q. et al. Evolution of charge density waves from three-dimensional to quasi-two-dimensional in kagome superconductors $Cs(V_{1-x}M_x)_3Sb_5$ (*M*=Nb, Ta). *Phys. Rev. Mater.* **7**, 074801 (2023).
21. Mu, C. et al. s-wave superconductivity in kagome metal CsV_3Sb_5 revealed by $^{121/123}$Sb NQR and ^{51}V NMR measurements. *Chinese Physics Letters* **38**, 077402 (2021).
22. Duan, W. et al. Nodeless superconductivity in the kagome metal CsV_3Sb_5. *Sci. China - Phys. Mech. Astron.* **64**, 107462 (2021).
23. Roppongi, M. et al. Bulk evidence of anisotropic s-wave pairing with no sign change in the kagome superconductor CsV_3Sb_5. *Nat. Commun.* **14**, 667 (2023).
24. Yin, L. et al. Strain-sensitive superconductivity in the kagome metals KV_3Sb_5 and CsV_3Sb_5 probed by point-contact spectroscopy. *Phys. Rev. B* **104**, 174507 (2021).
25. Gupta, R. et al. Microscopic evidence for anisotropic multigap superconductivity in the CsV_3Sb_5 kagome superconductor. *npj Quantum Materials* **7**, 49 (2022).
26. Zhong, Y. et al. Testing electron-phonon coupling for the superconductivity in kagome metal CsV_3Sb_5. *Nat. Commun.* **14**, 1945 (2023).
27. Feng, X., Jiang, K., Wang, Z. & Hu, J. Chiral flux phase in the Kagome superconductor AV_3Sb_5. *Sci. Bull.* **66**, 1384 – 1388 (2021).
28. Khasanov, R. et al. Time-reversal symmetry broken by charge order in CsV_3Sb_5. *Phys. Rev. Research* **4**, 023244 (2022).
29. Hu, Y.et al. Time-reversal symmetry breaking in charge density wave of CsV_3Sb_5 detected by polar Kerr effect. Preprint at *arXiv:2208.08036* (2022).
30. Mielke III, C. et al. Time-reversal symmetry-breaking charge order in a kagome superconductor. *Nature* **602**, 245–250 (2022).
31. Guguchia, Z. et al. Tunable unconventional kagome superconductivity in charge ordered RbV_3Sb_5 and KV_3Sb_5. *Nat. Commun.* **14**, 153 (2023).
32. Le, T. et al. Superconducting diode effect and interference patterns in kagome CsV_3Sb_5. *Nature* **630**, 64–69 (2024).
33. Saykin, D. R. et al. High resolution polar kerr effect studies of CsV_3Sb_5: tests for time-reversal symmetry breaking below the charge-order transition. *Phys. Rev. Lett.* **131**, 016901 (2023).
34. Wang, J., Farhang, C., Ortiz, B. R., Wilson, S. D. & Xia, J. Resolving the discrepancy between MOKE measurements at 1550-nm wavelength on kagome metal CsV_3Sb_5. *Phys. Rev. Mater.* **8**, 014202 (2024).
35. Herland, E. V., Babaev, E. & Sudbø, A. Phase transitions in a three dimensional U(1) × U(1) lattice London superconductor: metallic superfluid and charge-4*e* superconducting states. *Phys. Rev. B* **82**, 134511 (2010).
36. Zhou, S. & Wang, Z. Chern Fermi pocket, topological pair density wave, and charge-4e and charge-6e superconductivity in kagomé superconductors. *Nat. Commun.* **13**, 7288 (2022).
37. Hecker, M., Willa, R., Schmalian, J. & Fernandes, R. M. Cascade of vestigial orders in two-component superconductors: Nematic, ferromagnetic, *s*-wave charge-4*e*, and *d*-wave charge-4*e* states. *Phys. Rev. B* **107**, 224503 (2023).
38. Zhang, L.-F., Wang, Z. & Hu, X. Higgs-Leggett mechanism for the elusive 6e superconductivity observed in Kagome vanadium-based superconductors. Preprint at *arXiv:2205.08732*. (2022).
39. Ge, J. et al. Charge-4*e* and charge-6*e* flux quantization and higher charge superconductivity in kagome superconductor ring devices. *Phys. Rev. X* **14**, 021025 (2024).

40. Varma, C. M. & Wang, Z. Extended superconducting fluctuation region and 6e and 4e flux-quantization in a Kagome compound with a normal state of 3Q-order. Preprint at *arXiv:2307.00448*.(2023).
41. Nie, L. et al. Charge-density-wave-driven electronic nematicity in a kagome superconductor. *Nature* **604**, 59–64 (2022).
42. Asaba, T. et al. Evidence for an odd-parity nematic phase above the charge-density-wave transition in a kagome metal. *Nat. Phys.* **20**, 40–46 (2024).
43. Mühlbauer, S. et al. Magnetic small-angle neutron scattering. *Rev. Mod. Phys.* **91**, 015004 (2019).
44. White, J. *Handbook of Superconductivity, Characterization and Applications*, chap. Neutron Techniques: Flux-Line Lattice, 95–104 (CRC Press, 2021).
45. Levett, S. J., Dewhurst, C. D. & Paul, D. M. Vortex-lattice transitions in YNi_2B_2C: nature of the 45-degree reorientation. *Phys. Rev. B* **66**, 014515 (2002).
46. Li, J. et al. Strong-coupling superconductivity and weak vortex pinning in Ta-doped CsV_3Sb_5 single crystals. *Phys. Rev. B* **106**, 214529 (2022).
47. Huang, Z. et al. Tunable vortex bound states in multiband CsV_3Sb_5-derived kagome superconductors. *Sci. Bull.* **69**, 885–892 (2024).
48. Kogan, V. G. et al. Vortex lattice transitions in borocarbides. *Phys. Rev. B* **55**, R8693–R8696 (1997).
49. Franz, M., Affleck, I. & Amin, M. Theory of equilibrium flux lattices in unconventional superconductors. *Phys. Rev. Lett.* **79**, 1555–1558 (1997).
50. Agterberg, D. F. Square vortex lattices for two-component superconducting order parameters. *Phys. Rev. B* **58**, 14484–14489 (1998).
51. Ichioka, M., Hasegawa, A. & Machida, K. Field dependence of the vortex structure in *d*-wave and *s*-wave superconductors. *Phys. Rev. B* **59**, 8902–8916 (1999).
52. Hirano, T., Takamori, K., Ichioka, M. & Machida, K. Rotation of triangular vortex lattice in the two-band superconductor MgB_2. *J. Phys. Soc. Japan* **82**, 063708 (2013).
53. Ortiz, B. R. et al. Fermi surface mapping and the nature of charge-density-wave order in the kagome superconductor CsV_3Sb_5. *Phys. Rev. X* **11**, 041030 (2021).
54. Hu, Y. et al. Rich nature of Van Hove singularities in kagome superconductor CsV_3Sb_5. *Nat. Commun.* **13**, 2220 (2022).
55. Cubitt, R. et al. Effects of two-band superconductivity on the flux-line lattice in magnesium diboride. *Phys. Rev. Lett.* **91**, 047002 (2003).
56. Avers, K. E. et al. Broken time reversal symmetry in the topological superconductor UPt_3. *Nat. Phys.* **16**, 531–535 (2020).
57. Avers, K. E. et al. Effects of the order parameter anisotropy on the vortex lattice in UPt_3. *Front. Electron. Mater.* **2**, 878308 (2022).
58. Abrikosov, A. A. On the magnetic properties of superconductors of the second group. *Sov. Phys. JETP* **5**, 1174–1183 (1957).
59. Kemoklidze, M. P. Scattering of neutrons by quantized magnetic flux lines in type II superconductors. *Sov. Phys. JETP* **20**, 1505–1507 (1965).
60. Christen, D. K., Tasset, F., Spooner, S. & Mook, H. A. Study of intermediate mixed state of niobium by small-angle neutron-scattering. *Phys. Rev. B* **15**, 4506–4509 (1977).
61. Yaouanc, A., Dalmas de Réotier, P. & Brandt, E. H. Effect of the vortex core on the magnetic field in hard superconductors. *Phys. Rev. B* **55**, 11107–11110 (1997).
62. Eskildsen, M. R., Forgan, E. M. & Kawano-Furukawa, H. Vortex structures, penetration depth and pairing in iron-based superconductors studied by small-angle neutron scattering. *Rep. Prog. Phys.* **74**, 124504 (2011).
63. DeBeer-Schmitt, L. et al. Pauli paramagnetic effects on vortices in superconducting $TmNi_2B_2C$. *Phys. Rev. Lett.* **99**, 167001 (2007).
64. Bianchi, A. D. et al. Superconducting vortices in $CeCoIn_5$: toward the Paui-limiting field. *Science* **319**, 177–180 (2008).
65. White, J. S. et al. Observations of Pauli paramagnetic effects on the flux line lattice in $CeCoIn_5$. *New J. Phys.* **12**, 023026 (2010).
66. Brandt, E. H. The flux-line lattice in superconductors. *Rep. Prog. Phys.* **58**, 1465–1594 (1995).
67. Prozorov, R. & Giannetta, R. W. Magnetic penetration depth in unconventional superconductors. *Supercond. Sci. Technol.* **19**, R41–R67 (2006).
68. Gross, F. et al. Anomalous temperature-dependence of the magnetic-field penetration depth in superconducting UBe_{13}. *Z. Phys. B* **64**, 175–188 (1986).
69. Ritz, E. T. et al. Superconductivity from orbital-selective electron-phonon coupling in AV_3Sb_5. *Phys. Rev. B* **108**, L100510 (2023).
70. Ortiz, B. R. et al. New kagome prototype materials: discovery of KV_3Sb_5, RbV_3Sb_5 and CsV_3Sb_5. *Phys. Rev. Mater.* **3**, 094407 (2019).
71. Wang, Z. et al. Electronic nature of chiral charge order in the kagome superconductor CsV_3Sb_5. *Phys. Rev. B* **104**, 075148 (2021).
72. Dewhurst, C. D. Graphical reduction and analysis small-angle neutron scattering program: GRASP. *J. Appl. Crystallogr.* **56**, 1595–1609 (2023).
73. Xie, Y. et al. Conventional Superconductivity in the Doped Kagome Superconductor Cs(V0.86Ta0.14)3Sb5 from Vortex Lattice Studies. figshare. Dataset. https://doi.org/10.6084/m9.figshare.25737993.

Acknowledgements

The neutron scattering work was supported by the U.S. Department of Energy, Office of Basic Energy Sciences, under award no. DE-SC0005051 (N.C., M.R.E.) and no. DE-SC0012311 (Y.X, W.Y, P.D), and by the Swiss National Science Foundation (SNSF) Project grant 200021_188707 (J.S.W.). The single-crystal characterization efforts at Rice are supported by the Robert A. Welch Foundation Grant No. C-1839 (P.D.). The work at Beijing Institute of Technology (BIT) was supported by the National Key R&D Program of China Grants No. 2020YFA0308800 and 2022YFA1403400, and by the Beijing Natural Science Foundation Grant No. Z210006 (Z.W., J.L, Y.Y.). Z.W. thanks the Analysis & Testing Center at BIT for assistance in facility support. This work is based on experiments performed at the Swiss Spallation Neutron Source SINQ, Paul Scherrer Institute, Villigen, Switzerland. A portion of this research used resources at the High Flux Isotope Reactor, a DOE Office of Science User Facility operated by the Oak Ridge National Laboratory.

Author contributions

M.R.E., P.D., and J.-X.Y. conceived and designed the experiments. Y.X., N.C. W.Y., L.M.D.-S, J.S.W., P.D., and M.R.E. performed the experiments. Y.X. and N.C. analyzed the data. Z.W., J.L., and Y.Y. contributed materials/analysis tools. M.R.E., Y.X, N.C., and P.D. wrote the paper.

Competing interests

The authors declare no competing interests

Additional information

Supplementary information The online version contains supplementary material available at https://doi.org/10.1038/s41467-024-50856-2.

Correspondence and requests for materials should be addressed to Morten Ring Eskildsen.

Peer review information *Nature Communications* thanks Minghu Fang, and the other, anonymous, reviewer(s) for their contribution to the peer review of this work. A peer review file is available.